# Low-Velocity Zone in Smooth Pipe Culvert with and without Streamwise Rib for Fish Passage

Hubert Chanson[1]

**Abstract:** Unimpeded waterway connectivity is a requirement for all freshwater fish. While box culverts are considered the most effective design in terms of upstream fish passage, circular culverts are very common. Detailed hydrodynamic measurements were undertaken under controlled conditions in a near-full-scale smooth pipe culvert operating at less-than-design flows. Two configurations were tested: a smooth semicircular channel and a circular channel equipped with a small streamwise rib placed asymmetrically. For all investigated flow conditions, the channel flow was subcritical and corresponded to less-than-design conditions. Detailed measurements showed high velocities through the entire cross-section, with no obvious low-velocity region along the smooth wetted perimeter. The presence of an asymmetrical streamwise rib induced the formation of a small well-defined low-velocity zone (LVZ) in the vicinity of the rib. The flow resistance was slightly larger than that in a rectangular channel, for identical boundary roughness and flow conditions. The streamwise rib had a limited impact on the flow resistance, although large transverse gradient in skin friction shear stress, conducive of secondary currents, were observed. While the low-velocity zone size relevant to the upstream passage of small fish was smaller in the smooth circular channel than in a comparable rectangular channel, the introduction of the asymmetrical streamwise rib might create preferential swimming paths for small-bodied fish and juveniles of larger fish. The present physical results may serve as a validation data set for future computational fluid dynamics (CFD) modeling, to assist with the development of more efficient designs. **DOI: 10.1061/(ASCE)HY.1943-7900.0001789.** 

**Author keywords:** Fish passage; Hydrodynamics; Low-velocity zone (LVZ); Physical modeling; Smooth pipe culverts; Streamwise rib.

## Introduction

Although the impact of large hydraulic structures on stream ecology is well publicized, waterway crossings and culverts have often been ignored despite their major impact on fish passage (Anderson et al. 2012). Box culverts are considered a more effective design in terms of upstream fish passage (Briggs and Galarowicz 2013). But circular pipe culverts are the most common (Schall et al. 2012) (Fig. 1). The literature on pipe culvert hydraulics in relation to fish passage remains limited, except for some works on corrugated culverts (Abbs et al. 2007; Clark and Kehler 2011), partially-filled culverts (Clark et al. 2014), and baffled culverts (Olsen and Tullis 2013). A small number of relevant laboratory studies investigated smooth partially-filled pipe flows (Repogle and Chow 1966; Nalluri and Novak 1973; Sterling and Knight 2000) and semicircular channels (Kazemipour and Apelt 1980), while a CFD study included Wu et al. (2018).

While fish attraction and entrance into weirs and culverts have been recognized for sometimes as key factors for upstream fish passage (Pavlov 1999; Guiny et al. 2005; Haro et al. 2004), a number of recent studies discussed the current knowledge gaps, including the relationship between hydrodynamics and fish passage in culverts (Doering et al. 2011; Kemp 2012; Kerr et al. 2016; Wilkes et al. 2018). Beyond fish attraction at entrance, the manner in which waterway crossings block fish movement include an excessive vertical drop at the culvert exit, accumulation of debris and sediments at the culvert inlet in the barrel, standing waves in the outlet and inlet, and high velocity and insufficient water depth in the culvert barrel (Behlke et al. 1991; Olsen and Tullis 2013; Khodier and Tullis 2018), all of which being closely linked to the targeted fish species. Although the first three types of blockage may be remedied through proper construction, maintenance, and transition reshaping, respectively, high water velocities in the culvert barrel are often a major obstacle for successful upstream fish passage, in particular for small-bodied fish species and juveniles of larger fish (Pavlov et al. 2000; Neary 2012; Wang and Chanson 2018a). Field observations reported fish seeking low velocity zones associated with high turbulence intensity levels to pass through culvert barrels (Behlke et al. 1991; Blank 2008; Jensen 2014; Katopodis and Gervais 2016; Wang et al. 2016; Cabonce et al. 2019). The findings are consistent with basic theoretical energetic considerations (Lighthill 1960; Behlke et al. 1991; Wang and Chanson 2018b).

The current contribution aims to characterize the hydrodynamics of smooth pipe culverts operating at less-than-design flows, and to describe accurately the low velocity zone relevant to fish passage of small-bodied fish. This was undertaken through detailed hydrodynamic measurements in a near-full-scale pipe culvert barrel, although fish traversability was not tested. The present work is based upon the assumption that fishes need low-velocity zones (LVZs) to swim successfully upstream, because this has been widely recognized for small-bodied fish species and juvenile of large fish in channels (Pavlov et al. 2000; Wang et al. 2016; Cabonce et al. 2018). The study outcomes provide a better characterization of the LVZ and highlight a number of challenges to achieve successful upstream fish passage in smooth pipe culverts.

[1]Professor in Hydraulic Engineering, School of Civil Engineering, Univ. of Queensland, Brisbane, QLD 4072, Australia. ORCID: https://orcid.org/0000-0002-2016-9650. Email: h.chanson@uq.edu.au

Note. This manuscript was submitted on December 9, 2019; approved on April 8, 2020; published online on June 17, 2020. Discussion period open until November 17, 2020; separate discussions must be submitted for individual papers. This paper is part of the ***Journal of Hydraulic Engineering***, © ASCE, ISSN 0733-9429.


**Fig. 1.** Smooth pipe culverts: (a) single cell pipe culvert outlet in St Lucia Queensland (Australia) on January 20, 2019; and (b) three-cell pipe culvert outlet along Witton Creek, below Kate Street, Indooroopilly Queensland (Australia) on October15, 2018 at the end of rainstorm. (Images by author.)

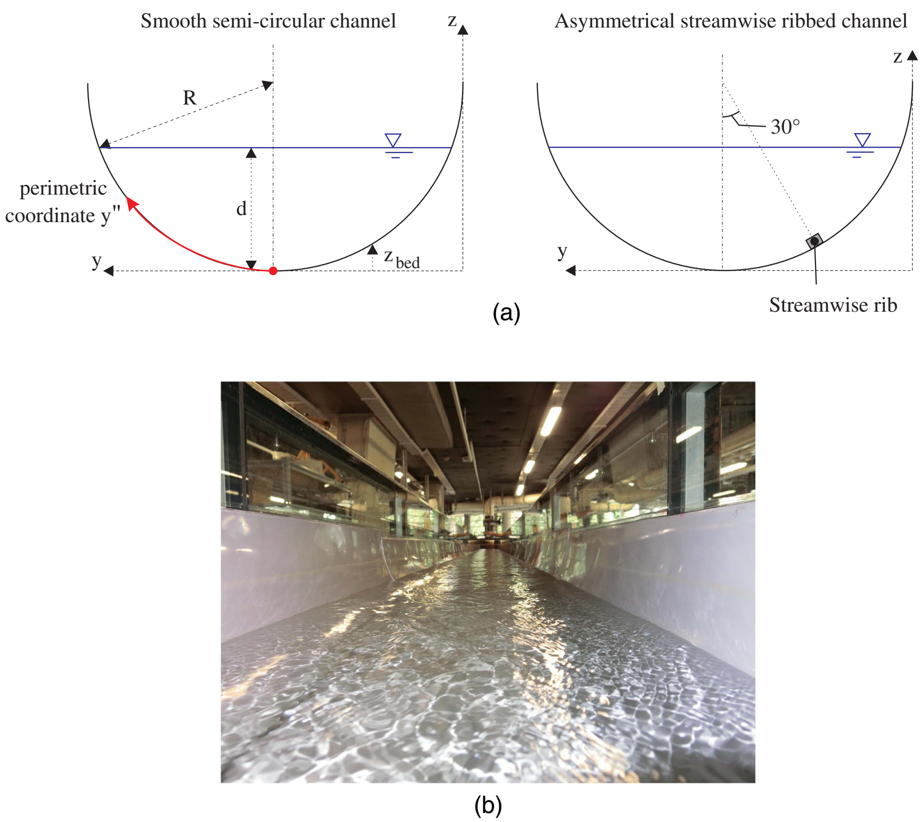


**Fig. 2.** Semicircular channel: (a) definition sketch, looking downstream; and (b) channel looking upstream of $Q = 0.015\ \mathrm{m^3/s}$.

## Experiments and Instrumentation

The experiments were performed in a 15-m-long 0.5-m-wide flume, set with a horizontal slope (Fig. 2). A semicircular invert, with an internal diameter of $D = 0.50$ m, was installed on the floor between $x = 1.17$ and 14.42 m, where $x$ is the longitudinal distance from the upstream end of the flume. The semicircular channel consisted of a number of 1-m-long semicircular sections made from 1.5-mm-thick PVC sheets. The PVC sheets were formed and glued on 12-mm-thick PVC ribs cut using a water jets with a tolerance of less than 0.5 mm. Each section is supported by 4 ribs, including one at each end, to guarantee no measureable deflection along the length and no change in the diameter of the half pipe under maximum load of water. A precise internal diameter of $D = 0.50$ m was fulfilled with a tolerance of less than 1 mm. A smooth transition section was installed between $x = 0.02$ and 1.17 m at the

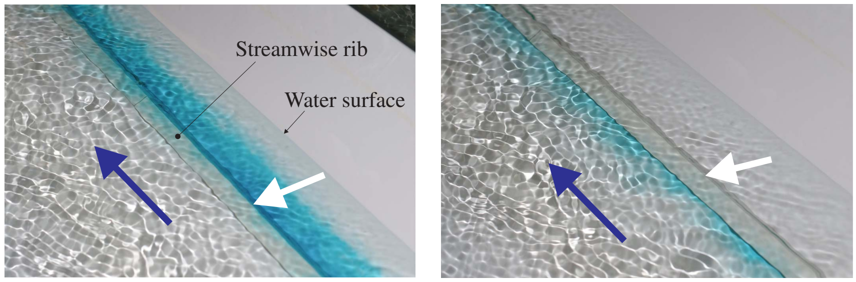


**Fig. 3.** Flow visualization and dye injection experiments in smooth flume with streamwise rib (white arrow). Note the coloured dye injected along the sides of rib, sticking to the rib and not mixing with the bulk of the flow. $R = 0.25$ m; $S_o = 0$; and $Q = 0.015$ $m^3/s$. Flow direction from bottom right to top left (thick dark arrow): (a) dye injection on the right of the rib; and (b) dye injection in the bottom left corner of the rib.

**Table 1.** Detailed laboratory studies of smooth circular open channels

| Reference | $S_o$ | $D$ (m) | $Q$ ($m^3/s$) | Re | Measurements |
|---|---|---|---|---|---|
| Repogle (1964) | — | 0.133 | 0.0014 to 0.0106 | $0.89 \times 10^4$ to $4.4 \times 10^4$ | Depth, velocity |
| Nalluri and Novak (1973) | 0.00007 to 0.0006 | 0.305 | — | $0.61 \times 10^5$ to $1.3 \times 10^5$ | Velocity |
| Kazemipour (1979) | 0.00052 | 0.379 | 0.0061 to 0.0160 | 0.73 to $1.35 \times 10^5$ | Depth, velocity |
| Sterling (1998) | 0.001 | 0.244 | 0.0054 to 0.0229 | $0.65 \times 10^5$ to $1.5 \times 10^5$ | Depth, velocity, boundary shear stress |
| Current study Series 1 | 0 | 0.50 | 0.015 to 0.055 | $1.27 \times 10^5$ to $3.48 \times 10^5$ | Depth, velocity, pressure, boundary shear stress |
| Current study Series 2[a] | — | — | 0.055 | $2.98 \times 10^5$ | — |

Note: $D$ = internal pipe diameter; $Q$ = water discharge; Re = Reynolds number defined in terms of hydraulic diameter; and $S_o$ = bed slope.
[a]Asymmetrical streamwise rib.

upstream end. The semicircular section (1.17 m $< x <$ 14.42 m) ended with a drop. Further downstream, the 15-m-long flume ended with a free overfall, located at $x = 15$ m. For a second series of experiments, a streamwise rib was installed along the semicircular invert at 30° from the centerline vertical [Fig. 2(a) and 3]. The rib was 30-mm wide, 20-mm high, and 12-m long. The purpose of the rib was to induce some flow asymmetry and to create a larger LVZ.

The discharge was measured with a Venturi meter (Brisbane, Australia) installed on the supply line with an accuracy within 2%. The free surface elevation was recorded with a pointer gauge within ±0.5 mm. The velocity and pressure were recorded with a Prandtl-Pitot tube (Dwyer 166 Series tube Ø3.18 mm, Dwyer Instruments, Michigan City, Indiana). The Prandtl-Pitot tube was further used as a Preston tube to record the skin friction, when the tube was in contact with the boundary. Based upon dimensional and theoretical considerations, the calibration followed closely an analytical solution of the Prandtl mixing length theory for smooth turbulent boundary (Cabonce et al. 2019). In addition, an acoustic Doppler velocimeter (ADV) Nortek (Norway) Vectrino+ equipped with a three-dimensional (3D) side-looking head was tested. A number of issues were recorded with the ADV data, as discussed by Chanson (2019a). Some ADV signal scattering was induced by the curved invert surface, especially next to the invert, with a systematic underestimate of the longitudinal velocities and a substantial reduction in number of good samples, correlation, and SNR, not unlike previous findings (Garner 2011). The vertical translation of the velocimeters was controlled by a fine adjustment traverse mechanism connected to a digital scale unit. The error on the vertical, transverse, and longitudinal position of the probe was $\Delta z < \pm 0.025$ mm, $\Delta y < \pm 1$ mm, and $\Delta x < \pm 2$ mm, respectively.

The experiments were performed in the horizontal semicircular channel, acting as a 0.5-m diameter full-scale pipe culvert barrel, operating with free-surface flows. The flow patterns and free-surface measurements were undertaken along the whole length of the flume for a relatively wide range of flow rates: 0.005 $m^3/s < Q <$ 0.055 $m^3/s$, which would correspond to less-than-design discharges. Detailed velocity measurements were undertaken for flow rates between 0.015 $m^3/s < Q <$ 0.055 $m^3/s$ at x = 2 m, 7.15 m and 12 m on the smooth invert, and for $Q = 0.055$ $m^3/s$ at $x = 7.15$ m in the presence of the asymmetrical streamwise rib (Table 1). The measurements were conducted at several transverse locations to characterize the 3D nature of the turbulent flow. Each vertical velocity profile consisted of a minimum of 25 points. At each cross-section, the number of velocity sampling points ranged from 181 to 323, with a larger number of points with increasing flow depth. The point velocity measurements nearest to the culvert invert were located approximately 1.6 mm from the boundary, while the Prandtl-Pitot tube was capable of taking measurements at or within 2 mm of the water surface. In addition, boundary shear stress measurements were conducted at each longitudinal location along the entire wetted perimeter, using the Prandtl-Pitot tube lying onto the channel invert. Table 1 details the experimental flow conditions for the velocity, pressure, and boundary shear stress measurements, and include past experimental studies in circular channels.

## Flow Patterns and Flow Resistance

For all investigated discharges, the water depth fulfilled $d/D < 0.5$, corresponding to a partially-filled pipe culvert operating for less than half full. The free-surface flow was subcritical in the



J. Hydraul. Eng., 2020, 146(9): 04020059

semicircular channel section; the water depth was greater than the critical flow depth: $d/d_c > 1$, where $d_c$ is the critical flow depth of the semicircular channel flow. The water surface was smooth with little surface roughness [Figs. 2(b) and 3]. Dye injection was conducted in the smooth invert configuration (Series 1). The visual observations showed a high velocity flow through the entire cross-section, with no obvious LVZ, associated to a very rapid diffusion of the dye in the channel. In presence of the streamwise rib (Series 2), visual observations and dye injection suggested that the rib presence induced elongated longitudinal eddies on both sides of the rib (Fig. 3). The dye injection showed limited mixing between the longitudinal helicoidal eddy flow alongside the rib and the main stream flow, as seen in [Figs. 3(a and b)], in which the colored dye remains in the close vicinity of the rib.

The free surface measurements showed that the water depth decreased with increasing streamwise coordinate, corresponding to a steady H2 backwater profile for all investigated flows (Henderson 1966; Chanson 2004). The data were analyzed to characterize the flow resistance of the semicircular channel based upon energy considerations and the best data fit between measured and calculated total head line slope. The results are presented in Fig. 4 and in Appendix. In Fig. 4, the present data (round empty symbols) are compared to previous circular open channel data (Kazemipour 1979; Sterling 1998) and to the Karman-Nikuradse formula for smooth turbulent flows (Henderson 1966; Chanson 2004). The flow resistance in the smooth semicircular channel was comparable to, although slightly larger than, that in a smooth rectangular channel for comparable flow conditions (Fig. 4). Fig. 4 compares the present flow resistance data with circular channel data with smooth and rough inverts. The present friction factor data were in agreement with other smooth circular channel configurations for similar Reynolds numbers (Fig. 4), although some data scatter was noted, especially at low flow rates. Altogether, all circular open channel flow resistance data were slightly larger than that of smooth turbulent pipe and boundary layer flows (Fig. 4, dashed thick line). The increased flow resistance was likely caused by some secondary motion induced by the circular channel shape and the associated turbulent dissipation (Kazemipour and Apelt 1980; Sterling and Knight 2000).

The flow resistance of the channel equipped with the asymmetrical rib (Series 2) was in average 15% smaller than that the smooth semicircular invert for comparable flow conditions (Fig. 4). It is hypothesized that the rib redirected the flow streamlines in its vicinity and altered the secondary motion and associated turbulent losses.

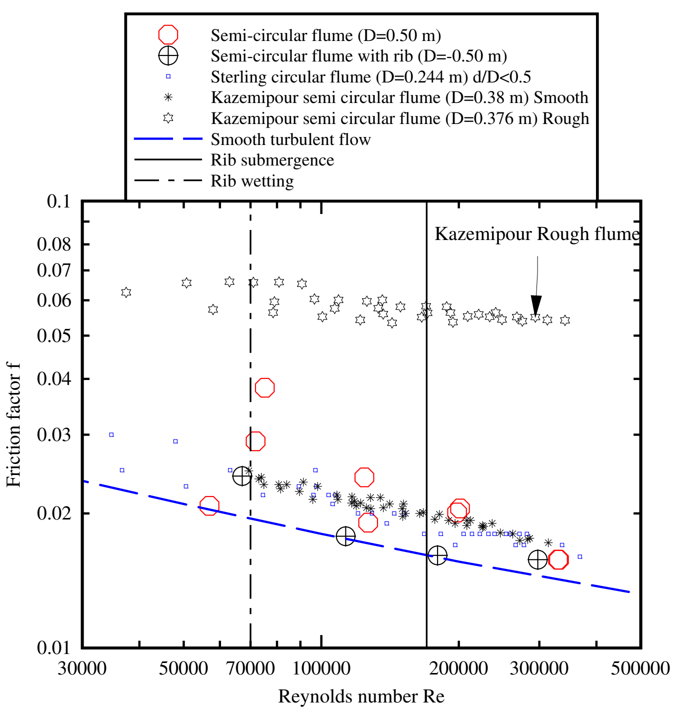


**Fig. 4.** Darcy–Weisbach friction factor of the semicircular channel without (Series 1) and with (Series 2) streamwise rib as a function of the Reynolds number. Comparison between present data (round symbols), previous circular open channel data, and the Karman-Nikuradse formula for smooth turbulent flows. (Data from Kazemipour 1979; Sterling 1998.)

## Velocity Distributions

In the smooth channel experiments (Series 1), large velocities were observed about the centerline of the flume as illustrated in Fig. 5, with $z$ the vertical distance, $y$ the transverse coordinate, $V_x$ the longitudinal velocity component, and $V_{\mathrm{mean}}$ the bulk velocity. At the upstream end of the channel ($x = 2.0$ m), the velocity was quasi-uniform with a small boundary layer region (Chanson 2019a). Further downstream, the velocity field were fully-developed and the boundary effects extended to the entire flow cross-section area. The data showed some impact of the relative water depth $d/D$, hence the water discharge, on the velocity distributions. In the fully-developed flow region, all the velocity data presented a very thin region next to the invert with a marked velocity gradient, as previously reported (Repogle 1964; Nalluri and Novak 1973; Sterling 1998). The centerline data compared favorably to the theoretical log-wake law velocity distribution and the no-slip boundary condition at the invert, i.e., $V_x(z = z_{\mathrm{bed}}) = 0$. With the streamwise rib (Series 2), the vertical velocity data indicated some flow asymmetry, as well as some low velocity zone in the close proximity of the rib.

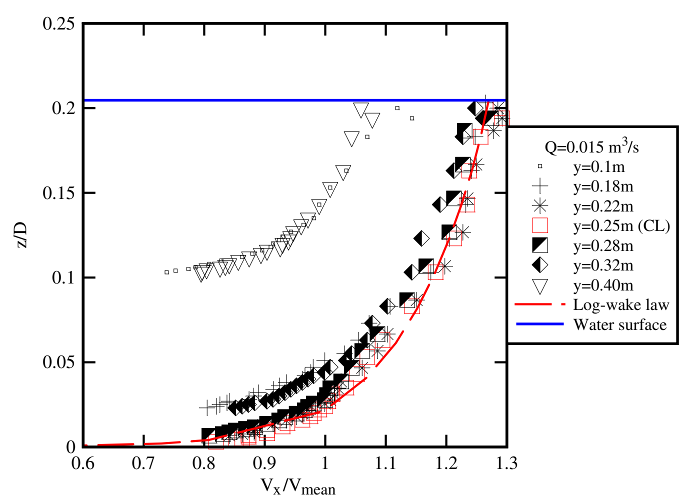


**Fig. 5.** Vertical profiles of dimensionless longitudinal velocity component $V_x/V_{\mathrm{mean}}$ in the smooth semicircular channel (Series 1) at several transverse locations. $Q = 0.015$ m$^3$/s; $D = 0.5$ m; $d = 0.102$ m; and $V_{\mathrm{mean}} = 0.519$ m/s. Centerline data ($y = 0.25$ m) are compared with log-wake law.

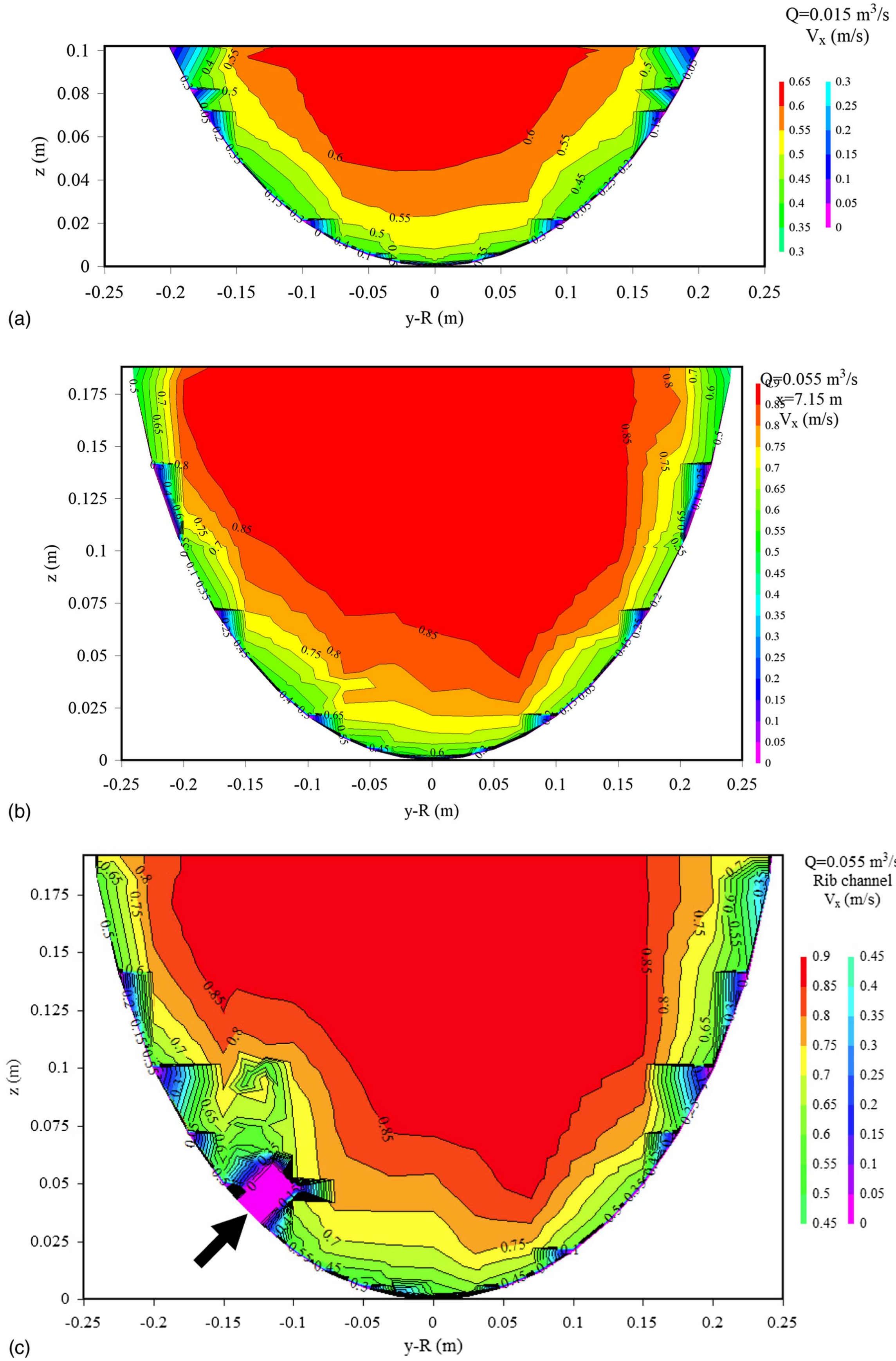


**Fig. 6.** Longitudinal velocity contour maps in the semicircular channel at $x = 7.15$ m. Comparison between smooth and ribbed channel data. Legend indicate the longitudinal velocity $V_x$ in m/s: (a) $Q = 0.015\ \mathrm{m^3/s}$, $D = 0.5$ m, $d = 0.102$ m, and $V_{\mathrm{mean}} = 0.519$ m/s (Series 1); (b) $Q = 0.055\ \mathrm{m^3/s}$, $D = 0.5$ m, $d = 0.188$ m, and $V_{\mathrm{mean}} = 0.815$ m/s (Series 1); and (c) $Q = 0.055\ \mathrm{m^3/s}$, $D = 0.5$ m, $d = 0.194$ m, and $V_{\mathrm{mean}} = 0.791$ m/s [Series 2, streamwise rib (black arrow)].

The longitudinal velocity contour maps indicated some large velocity gradients next to the entire wetted perimeter (Fig. 6). For the smallest discharge (i.e., $d_c/D = 0.16$), the data presented a pseudo-two-dimensional (2D) region located symmetrically around the centerline $[-0.2 < (y - D/2)/D < 0.2]$ where the iso-velocity contour lines were almost parallel to the horizontal, implying a quasi-2D flow region. For larger flow rates, the iso-velocity contour lines were more curved and the flow was 3D across the entire cross-sectional area (Fig. 6). The position where the maximum velocity occurred tended to take place slightly below the free-surface, e.g., at $0.8 < z/d < 1$. This phenomenon is believed to be linked to intense secondary motion and transverse momentum exchange (Liggett et al. 1965). The current data suggested that momentum is being transported towards the channel sides, even at low flows. Herein, the ratio of free-surface velocity to maximum velocity ranged from 0.98 to 1, for all flow conditions and all transverse locations. The cross-sectional maximum velocity data $(V_{\max})_M$ are reported in Appendix I (10th row). For the current study, the dimensionless maximum velocity data $(V_{\max})_M/V_{\text{mean}}$ decreased monotonically from 1.3 down to 1.15 with increasing relative depth $d/D$ between 0.2 and 0.37. The results were qualitatively and quantitatively close to the observations of Kazemipour (1979) in a smooth semicircular channel.

The presence of the small longitudinal rib induced a substantial modification of the velocity field next to the rib [Fig. 6(c)], especially for $0 < z < 0.1$ m and $-0.18$ m $< (y - D/2) < -0.05$ m. The rib had little influence on the bulk of the flow, including the cross-sectional maximum velocity and bulk velocity, although it generated locally some reduced velocity zone.

The velocity data were checked in terms of the conservation of mass. The velocity contour plots were integrated to yield the cross sectional flow rate

$$<Q> = \int_A V_x dA \tag{1}$$

where $<Q>$ = water discharge calculated by integrating the longitudinal velocity distribution across the flow cross-section area $A$. The results were in close agreement with the discharge measurements (Appendix I). In the smooth semicircular channel (Series 1), the difference between Eq. (1) and the measured discharge was 1%, 4.3%, and 1% for $Q = 0.015$, 0.028, and 0.055 $\text{m}^3/\text{s}$, respectively, at $x = 7.15$ m.

## Velocity Correction Coefficients

The complete velocity maps were integrated to give the velocity correction coefficients commonly used in one-dimensional (1D) flow modeling (Henderson 1966; Chanson 2004). Namely the momentum correction coefficient $\beta$ and the kinetic energy correction coefficient $\alpha$ defined as

$$\beta = \frac{\int_A \rho V_x^2 dA}{\rho V_{\text{mean}}^2 A} \tag{2}$$

$$\alpha = \frac{\int_A \rho V_x^3 dA}{\rho V_{\text{mean}}^3 A} \tag{3}$$

Both velocity correction factors were largely influenced by the relative depth and cross-sectional shape. The data showed large variations in trend, not unlike the findings of Repogle (1964) and Sterling (1998). The experimental results are reported in Appendix.

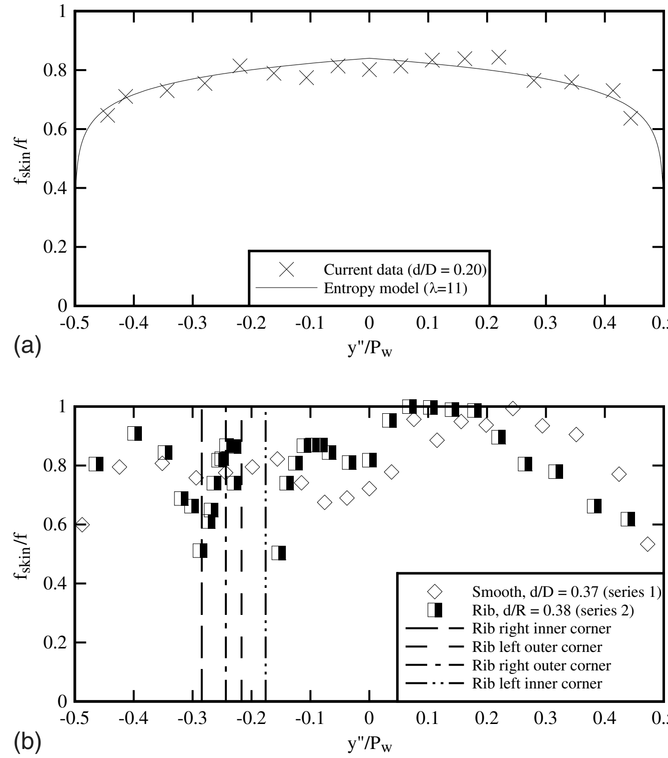


**Fig. 7.** Distributions of dimensionless boundary shear stress $f_{\text{skin}}/f$ along the wetted perimeter of semicircular channel: (a) data for $Q = 0.015$ $\text{m}^3/\text{s}$ at $x = 7.15$ m, compared to the entropy model (Eq. (7)); and (b) comparison between smooth and ribbed semicircular channels: $Q = 0.055$ $\text{m}^3/\text{s}$ and $x = 7.15$ m. Rib edges are indicated with vertical lines.

## Boundary Shear Stress Measurements

Boundary shear stress measurements were performed along the wetted perimeter, using the Prandtl-Pitot tube acting as a Preston tube. Fig. 7 presents typical distributions of dimensionless skin friction boundary shear stress along the wetted perimeter, where $f_{\text{skin}}$ is the dimensionless skin friction shear stress, $f$ is the dimensionless total boundary shear stress, $P_w$ is the wetted perimeter, and $y$" is the perimetric coordinate [Fig. 2(a)]. Fig. 2(a) (Left) shows the definition of the wetted perimeter coordinate $y$", with its origin on the channel centerline. In the smooth channel (Series 1), all the distributions were relatively flat, with a near-constant boundary shear across a large proportion of the wetted perimeter either side of the centerline. As the water depth and discharge increased, the shear stress distributions became less uniform. A noteworthy feature of all transverse distributions was the relatively high value of boundary shear stress next the water-air interface. This value was typically greater than 60% of the total boundary shear stress. Physically, the boundary shear stress was nonzero at the edge of the wetted perimeter, because the water in contact with the channel boundary creates a strong transverse gradient.

In the ribbed channel (Series 2), the skin friction data presented an asymmetrical transverse shape with large transverse variations in the vicinity of the rib, i.e., $-0.35 < y''/P_w < -0.1$ in Fig. 7(b), owing to the presence of the rib at 30° from the centerline.



J. Hydraul. Eng., 2020, 146(9): 04020059

The transverse profile hinted the existence of longitudinal vortical structures along the streamwise rib, consistent with dye injection (Fig. 3). Minimum shear stresses were observed next to the bottom inner corners of the rib.

## Comments

For both smooth and ribbed semicircular channels, the skin friction boundary shear stress was less than the total boundary shear stress: i.e., $f_{\mathrm{skin}}/f < 1$ (Fig. 7). The skin friction shear stress distributions were integrated along the wetted perimeter, to provide the cross-sectional averaged skin friction boundary shear stress

$$<(\tau_{\mathrm{o}})_{\mathrm{skin}}> = \frac{1}{\mathrm{P_w}} \int_{\mathrm{P_w}} (\tau_{\mathrm{o}})_{\mathrm{skin}} \mathrm{d}y'' \tag{4}$$

The data are summarized in terms of the dimensionless shear stress $<f_{\mathrm{skin}}> = <(\tau_{\mathrm{o}})_{\mathrm{skin}}>/(\rho V_{\mathrm{mean}}^2/8)$ in Appendix I. Depending upon the flow rate, the ratio of mean skin friction resistance to total flow resistance $<f_{\mathrm{skin}}>/f$ ranged from 0.35 to 0.66 (Appendix I).

The transverse distribution of boundary shear stress was compared to a method based on maximizing the entropy of the boundary shear stress (Sterling 1998). The analytical solution for a circular channel is

$$\frac{(\tau_{\mathrm{o}})_{\mathrm{skin}}}{((\tau_{\mathrm{o}})_{\mathrm{skin}})_{\mathrm{M}}} = \frac{1}{\lambda} \mathrm{Ln}\left(1 + (e^{\lambda} - 1)\left|1 - \frac{2y''}{\mathrm{P_w}}\right|\right) \tag{5}$$

where $((\tau_{\mathrm{o}})_{\mathrm{skin}})_M$ = maximum local skin friction boundary shear stress at the cross-section; $\lambda$ = Lagrange multiplier; and $y''$ = perimetric coordinate. Eq. (5) is compared to experimental observations in Fig. 7(a) with $\lambda$ selected based upon the best data fit. Herein $\lambda$ was found to be within 11 to 12 for the smooth invert configuration (Series 1). While Eq. (5) has been successfully applied to the smooth semicircular open channel flows, the physical interpretation of the parameter $\lambda$ is presently not possible. Sterling (1998) discussed two intrinsic limitations of the entropy method, namely the inability to reproduce the effects of secondary flows and the assumption of zero boundary shear stress at the free-surface.

## Discussion

In a semicircular channel, secondary flows are directed at right angle with the longitudinal flow direction, redistributing momentum across the channel (Liggett et al. 1965; Naot and Rodi 1982). The interactions between the transverse shear gradient along the wetted perimeter [Fig. 7(a)] and longitudinal flow motion induce energy losses, which must be compensated by some transverse secondary flow motion. In presence of the streamwise rib, the skin friction boundary shear stress was not symmetrically distributed about the channel centreline [Fig. 7(b)]. Large boundary shear stresses were recorded along the faces of the rib, with maximum shear stresses typically observed next to the external corners, which might be related to local fluid acceleration and streamwise vorticity. Such large skin friction shear stresses might suggest a region of strong interactions between the main flow, secondary currents and cavity recirculation, in a manner similar to observations on heterogeneous transverse roughness (Tominaga and Nezu 1991).

The current data showed regions of contrasted longitudinal velocities. The velocity field was analyzed in terms of the relative size of LVZ. The results are shown in Fig. 8(a) and Appendix I, as the fraction of flow area where the ratio of longitudinal velocity

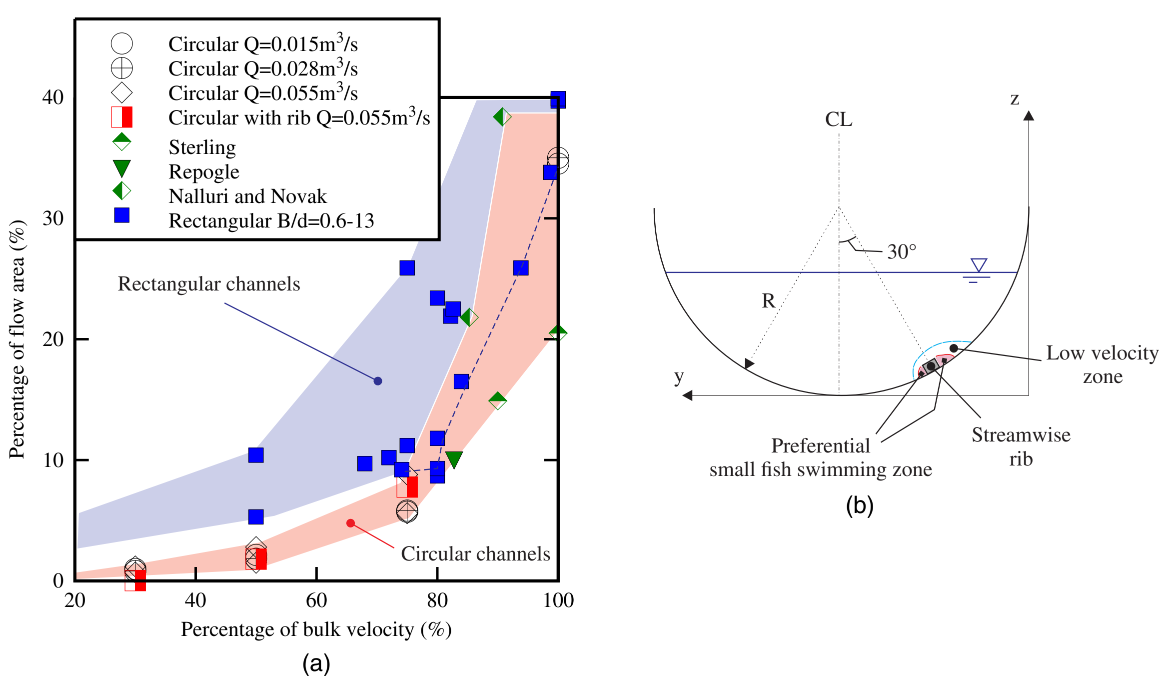


**Fig. 8.** LVZ in smooth pipe culvert: (a) fractions of LVZs where $V_x/V_{\mathrm{mean}}$ is less than a set value, for different discharges. Comparison between the present data at $x = 7.15$ m, smooth rectangular channel data, and smooth circular channel data. The dashed thin line shows the outer edge of the rectangular culvert data area and the white solid line marks the shows the outer edge of the pipe culvert data area (data from Nikuradse 1926; Nezu and Rodi 1985; Macintosh 1990; Xie 1998; Wang et al. 2018; Cabonce et al. 2019; Repogle 1964; Sterling 1998); and (b) sketch of LVZ and preferential fish swimming path in a circular channel with an asymmetrical streamwise rib.

to mean velocity $V_x/V_{mean}$ was less than 0.3, 0.5, 0.75, and 1. Altogether, the size of the LVZ was small in semicircular channels, and comparatively smaller than in smooth rectangular channels [Fig. 8(a)]. The present data compared reasonably favorably to earlier studies in smooth circular channels (Repogle 1964; Nalluri and Novak 1973; Sterling 1998). All the smooth circular channel data [Fig. 8(a), dark shaded area] showed substantially smaller low velocity zones, for the same range of flow conditions, than in smooth rectangular channels [Fig. 8(a), light shaded data]. Further the smooth pipe culvert data corresponded to a smaller LVZ than in roughened and corrugated pipe culverts (Kazemipour 1979; Ead et al. 2000; Abbs et al. 2007).

In presence of the asymmetrical streamwise rib, the velocity field showed a well-defined low velocity region next to the rib [Figs. 6(c) and 8(b)], while the high velocity regions tended to be skewed towards the smooth channel section. For $Q = 0.055\ m^3/s$, the $20 \times 30$ mm rib induced an LVZ about 50-mm wide and 100-mm deep. The sharp corners of the rib created hydrodynamic singularities, strong turbulence, transverse gradients in boundary shear stress [Fig. 7(b)] conducive of secondary currents, and local turbulent dissipation (Chanson 2019b). Both dye injection and velocity measurements showed the existence of longitudinal reduced velocity zones on both sides of the rib [Figs. 3 and 8(b)], which might constitute preferential fish swimming path, although this would need to be tested in a full-scale prototype structure.

## Conclusion

While box culverts are considered more effective for upstream fish passage, circular culverts are very common. In the current study, detailed physical measurements were performed in a near-full-scale smooth pipe culvert ($D = 0.50$ m) operating at less-than-design subcritical flows ($d/D < 0.5$). The thrust of the works was to characterize the LVZ, and to document the impact of a small appurtenance, i.e., a small streamwise rib placed asymmetrically.

The open channel flow was subcritical for all investigated flow conditions. Visual observations and detailed velocity measurements showed large velocities through the entire cross-section, with high-velocity gradient next to the whole invert and no obvious low-velocity region in the smooth circular channel. The flow resistance was slightly larger than that in a rectangular channel, for identical boundary roughness and flow conditions, likely as a consequence of the secondary motion induced by the circular channel shape. The streamwise rib had a limited impact on the flow resistance, although large transverse gradient in skin friction shear stress were recorded. The rib corners created flow singularities associated with strong turbulence, transverse gradients in shear stress conducive of secondary currents and local turbulent dissipation. For both smooth and ribbed semicircular channels, the skin friction boundary shear stress was less than the total boundary shear stress: i.e., $<f_{skin}>/f$ ranged from 0.55 to 0.66 at $x = 7.15$ m.

While the LVZ size relevant to the upstream passage of small fish was smaller in the smooth circular channel than in a comparable rectangular channel, the introduction of the asymmetrical streamwise rib might create preferential swimming paths for small-bodied fish and juveniles of larger fish. Although this hypothesis would need to be tested in a full-scale prototype structure, the present physical results deliver a validation data set for future computational fluid dynamics (CFD) modeling. Detailed and properly-validated CFD modeling could assist with the development of more efficient designs, although the optimum type of boundary treatment might be closely linked to the targeted fish species.

## Appendix. Summary of velocity data in smooth semicircular channel

| Parameter | Smooth circular channel (Series 1) | | | | | Asymmetrical streamwise rib (Series 2) |
|---|---|---|---|---|---|---|
| $Q$ (m$^3$/s) = | 0.015 | 0.028 | 0.055 | 0.055 | 0.055 | 0.055 |
| $d_c$ (m) = | 0.0802 | 0.1103 | 0.1672 | 0.1672 | 0.1672 | 0.1672 |
| $x$ (m) = | 7.15 | 7.15 | 2.0 | 7.15 | 12.0 | 7.15 |
| $d$ (m) = | 0.102 | 0.140 | 0.2035 | 0.188 | 0.172 | 0.194 |
| $A$ (m$^2$) = | 0.0289 | 0.045 | 0.0751 | 0.0675 | 0.0598 | 0.0696 |
| $B$ (m) = | 0.403 | 0.449 | 0.491 | 0.484 | 0.475 | 0.487 |
| $P_w$ (m) = | 0.469 | 0.555 | 0.434 | 0.660 | 0.623 | 0.733 |
| $V_{mean}$ (m/s) = | 0.519 | 0.622 | 0.733 | 0.815 | 0.919 | 0.791 |
| $Re$ = | $1.27 \times 10^5$ | $1.98 \times 10^5$ | $3.16 \times 10^5$ | $3.31 \times 10^5$ | $3.49 \times 10^5$ | $2.98 \times 10^5$ |
| $(V_{max})_M$(m/s) = | 0.671 | 0.799 | 0.847 | 0.943 | 1.086 | 0.921 |
| $<Q>$(m$^3$/s) = | 0.0148 | 0.0268 | 0.0570 | 0.0556 | 0.0537 | 0.0522 |
| $\alpha$ = | 1.310 | 1.280 | 1.218 | 1.137 | 1.060 | 0.9967 |
| $\beta$ = | 1.155 | 1.34 | 1.121 | 1.066 | 1.002 | 0.9289 |
| $f$ = | 0.0191 | 0.0201 | 0.0158 | 0.0155 | 0.0157 | 0.016 |
| $<f_{skin}>/f$ = | 0.66 | 0.57 | 0.35 | 0.58 | 0.35 | 0.55 |
| LVZ area with | | | | | | |
| $V_x < 0.3 \cdot V_{mean}$ | 0.99% | 0.66% | — | 0.83% | — | 0.04% |
| $V_x < 0.5 \cdot V_{mean}$ | 2.16% | 1.51% | — | 1.84% | — | 1.80% |
| $V_x < 0.75 \cdot V_{mean}$ | 5.72% | 5.56% | — | 5.82% | — | 7.77% |
| $V_x < V_{mean}$ | 34.5% | 44.6% | — | 35.0% | — | 51.4% |

Note: $A$ = cross-sectional area; $D = 0.50$ m; $d$ = water depth; $f$ = Darcy-Weisbach friction factor; $<f_{skin}>$ = dimensionless wetter perimeter average skin friction; LVZ = low velocity zone area relative the flow cross-section area; $P_w$ = wetted perimeter; $Q$ = water discharge; $<Q>$ = discharge calculated by integrating the longitudinal velocity data across the flow cross-sectional area; $S_o = 0$; $(V_{max})_M$ = cross-sectional maximum velocity; $V_{mean}$ = bulk velocity; $x$ = longitudinal coordinate; $a$ = kinetic energy correction coefficient; and $b$ = momentum correction coefficient.

## Data Availability Statement

Some or all data, models, or code that support the findings of this study are available from the corresponding author upon reasonable request. These include the tabular data corresponding to the data presented in Figs. 4–8(a). Further information is reported in Chanson (2019a).


## Acknowledgments

The author thanks his students Thomas Ward and Max Van Heeckeren who performed the experimental measurements, and Dr Xinqian (Sophia) Leng for her input into the project and her commentaries. He further thanks the anonymous reviewers for the constructive nature of their review comments. He acknowledges the technical assistance of Jason Van Der Gevel and Stewart Matthews (The University of Queensland). The financial support through the Queensland Department of Transport and Main Roads (TMTHF1805) and the School of Civil Engineering at the University of Queensland is acknowledged.


## Notation

*The following symbols are used in this paper:*

$A$ = channel cross-section area ($m^2$);
$B$ = free-surface width (m);
(b) = dimensionless boundary shear stress;
$D$ = internal pipe diameter (m);
$d$ = water depth (m);
$d_c$ = critical flow depth (m);
$f$(a) = Darcy-Weisbach friction factor;
$f_{skin}$ = skin friction factor measured with a Prandtl-Pitot tube lying on the bed;
$<f_{skin}>$ = wetted-perimeter-averaged skin friction factor measured with a Preston tube lying on the bed:

$$<f_{skin}> = \frac{\int_{P_w} (\tau_o)_{skin} dy''}{\frac{1}{8}\rho V_{mean}^2};$$

$g$ = gravity acceleration ($m/s^2$): $g = 9.80\,m/s^2$ in Brisbane, Australia;
LVZ = relative low-velocity zone cross-section area, where $0 < V_x < U_{fish}$, in the pipe culvert;
$P_w$ = wetted perimeter (m);
$Q$ = water discharge ($m^3/s$);
$<Q>$ = water discharge calculated by integrating the longitudinal velocity distribution across the flow cross-section area $A$:

$$<Q> = \int_A V_x dA;$$

Re = Reynolds number defined in terms of the hydraulic diameter;
$V_{max}$ = maximum velocity (m/s);
$V_{mean}$ = cross-sectional mean velocity (m/s): $V_{mean} = Q/A$;
$V_x$ = longitudinal velocity component (m/s);
$x$ = longitudinal distance (m) positive downstream measured from the upstream end of channel;
$y$ = transverse distance (m) measured from the right sidewall;
$y''$ = transverse coordinate (m) following the wetted perimeter, with $y'' = 0$ at the lowest invert elevation (i.e., channel bottom);
$z$ = elevation (m) above the lowest invert point;
$z_{bed}$ = invert elevation (m) above the datum;
$\alpha$ = kinetic energy correction coefficient, also called the Coriolis coefficient:

$$\alpha = \frac{\int_A \rho V_x^3 dA}{\rho V_{mean}^3 A};$$

$\beta$ = momentum correction coefficient, also called the Boussineq coefficient:

$$\beta = \frac{\int_A \rho V_x^2 dA}{\rho V_{mean}^2 A};$$

$\lambda$ = Lagrange multiplier;
$\rho$ = water density ($kg/m^3$);
$\tau_o$ = boundary shear stress (Pa);
$(\tau_o)_{skin}$ = local skin friction boundary shear stress (Pa) measured with a Preston tube lying on the bed;
$((\tau_o)_{skin})_M$ = maximum local skin friction boundary shear stress (Pa) at a cross-section;
$<(\tau_o)_{skin}>$ = wetted-perimeter-averaged skin friction boundary shear stress (Pa) measured with a Preston tube lying on the bed:

$$<(\tau_o)_{skin}> = \frac{1}{P_w}\int_{P_w} (\tau_o)_{skin} dy''; \text{ and}$$

Ø = diameter (m).

### Subscript

$c$ = critical flow conditions;
$M$ = cross-sectional maximum value;
max = maximum value in a vertical profile;
skin = skin friction; and
$x$ = longitudinal component.


## References

Abbs, T. J., J. A. Kells, and C. Katopodis. 2007. "A model study of the hydraulics related to fish passage through backwatered culverts." In *Proc., 18th Canadian Hydrotechnical Conf.*, 22–24. Montreal: Canadian Society of Civil Engineers.

Anderson, G. B., M. C. Freeman, B. J. Freeman, C. A. Straight, M. M. Hagler, and J. T. Peterson. 2012. "Dealing with uncertainty when assessing fish passage through culvert road crossings." *Environ. Manage.* 50 (3): 462–477. https://doi.org/10.1007/s00267-012-9886-6.

Behlke, C. E., D. L. Kane, R. F. McLeen, and M. T. Travis. 1991. *Fundamentals of culvert design for passage of weak-swimming fish*. Rep. No. FHWA-AK-RD-90-10. Juneau, AK: DOT and Public Facilities.

Blank, M. D. 2008. "Advanced studies of fish passage through culverts: 1-D and 3-D hydraulic modelling of velocity, fish energy expenditure, and a new barrier assessment method." Ph.D. thesis, Dept. of Civil Engineering, Montana State Univ.

Briggs, A. S., and T. L. Galarowicz. 2013. "Fish passage through culverts in central michigan warmwater streams." *North Am. J. Fish. Manage.* 33 (3): 652–664. https://doi.org/10.1080/02755947.2013.788589.

Cabonce, J., R. Fernando, H. Wang, and H. Chanson. 2019. "Using small triangular baffles to facilitate upstream fish passage in standard box culverts." *Environ. Fluid Mech.* 19 (1): 157–179. https://doi.org/10.1007/s10652-018-9604-x.

Cabonce, J., H. Wang, and H. Chanson. 2018. “Ventilated corner baffles to assist upstream passage of small-bodied fish in box culverts.” *J. Irrig. Drain. Eng.* 144 (8): 0418020. https://doi.org/10.1061/(ASCE)IR.1943-4774.0001329.

Chanson, H. 2004. *The hydraulics of open channel flow: An introduction*. 2nd ed. Oxford, UK: Butterworth-Heinemann.

Chanson, H. 2019a. *Physical modelling of semi-circular channels and low velocity zones—Application to pipe culverts and upstream fish passage at less-than-design flows*. Rep. No. CH116/19. Brisbane, Australia: School of Civil Engineering, Univ. of Queensland.

Chanson, H. 2019b. “Utilising the boundary layer to help restore the connectivity of fish habitats and populations: An engineering discussion.” *Ecol. Eng.* 141 (Dec): 105613. https://doi.org/10.1016/j.ecoleng.2019.105613.

Clark, S. O., J. S. Toews, and R. Tkach. 2014. “Beyond average velocity: Modelling velocity distributions in partially filled culverts to support fish passage guidelines.” *Int. J. River Basin Manage.* 12 (2): 101–110. https://doi.org/10.1080/15715124.2013.879591.

Clark, S. P., and N. Kehler. 2011. “Turbulent flow characteristics in circular corrugated culverts at mild slopes.” *J. Hydraul. Res.* 49 (5): 676–684. https://doi.org/10.1080/00221686.2011.596399.

Doering, K., R. G. Young, and A. R. McIntosh. 2011. “Factors affecting juvenile galaxiid fish passage at culverts.” *Mar. Freshwater Res.* 62 (1): 38–45. https://doi.org/10.1071/MF10101.

Ead, S. A., N. Rajaratnam, and C. Katopodis. 2000. “Turbulent open-channel flow in circular corrugated culverts.” *J. Hydraul. Eng.* 126 (10): 750–757. https://doi.org/10.1061/(ASCE)0733-9429(2000)126:10(750).

Garner, M. E. 2011. “Model study of the hydraulics related to fish passage through embedded culverts.” Master’s thesis, Dept. of Civil and Geological Engineering, Univ. of Sakatchewan.

Guiny, E., D. A. Ervine, and J. D. Amstrong. 2005. “Hydraulic and biological aspects of fish passes for Atlantic salmon.” *J. Hydraul. Eng.* 131 (7): 542–553. https://doi.org/10.1061/(ASCE)0733-9429(2005)131:7(542).

Haro, A., T. Castro-Santos, J. Noreika, and M. Odeh. 2004. “Swimming performance of upstream migrant fishes in open-channel flow: A new approach to predicting passage through velocity barriers.” *Can. J. Fish. Aquat. Sci.* 61 (9): 1590–1601. https://doi.org/10.1139/f04-093.

Henderson, F. M. 1966. *Open channel flow*. New York: MacMillan Company.

Jensen, K. M. 2014. “Velocity reduction factors in near boundary flow and the effect on fish passage through culverts.” M.Sc. thesis, Dept. of Civil and Environmental Engineering, Brigham Young Univ.

Katopodis, C., and R. Gervais. 2016. *Fish swimming performance database and analyses*. DFO CSAS Research Document No. 2016/002. Ottawa: Canadian Science Advisory Secretariat.

Kazemipour, A. K. 1979. “Cross-sectional shape effects on resistance to uniform flow in open channels and non-circular closed conduits.” Ph.D. thesis, Dept. of Civil Engineering, Univ. of Queensland.

Kazemipour, A. K., and C. J. Apelt. 1980. *Shape effects on resistance to flow in smooth semi-circular channels*. Research Rep. No. CE18. Brisbane, Australia: Univ. of Queensland.

Kemp, P. 2012. “Bridging the gap between fish behaviour, performance and hydrodynamics: An Ecohydraulics approach to fish passage research.” *River Res. Appl.* 28 (4): 403–406. https://doi.org/10.1002/rra.1599.

Kerr, J. R., C. Manes, and P. S. Kemp. 2016. “Assessing hydrodynamic space use of brown trout, Salmo trutta, in a complex flow environment: A return to first principles.” *J. Exp. Biol.* 219 (21): 3480–3491. https://doi.org/10.1242/jeb.134775.

Khodier, M. A., and B. P. Tullis. 2018. “Experimental and computational comparison of baffled-culvert hydrodynamics for fish passage.” *J. Appl. Water Eng. Res.* 6 (3): 191–199. https://doi.org/10.1080/23249676.2017.1287018.

Liggett, J. A., C. L. Chiu, and L. S. Miao. 1965. “Secondary currents in a corner.” *J. Hydraul. Div.* 91 (6): 99–117.

Lighthill, M. J. 1960. “Note on the swimming of slender fish.” *J. Fluid Mech.* 9 (2): 305–317. https://doi.org/10.1017/S0022112060001110.

Macintosh, J. C. 1990. “Hydraulic characteristics in channels of complex cross-section.” Ph.D. thesis, Dept. of Civil Engineering, Univ. of Queensland.

Nalluri, C., and P. Novak. 1973. “Turbulence characteristics in a smooth open channel of circular cross-section.” *J. Hydraul. Res.* 11 (4): 343–368. https://doi.org/10.1080/00221687309499768.

Naot, D., and W. Rodi. 1982. “Calculation of secondary currents in channel flow.” *J. Hydraul. Div.* 108 (8): 948–967.

Neary, V. S. 2012. “Binary fish passage models for uniform and nonuniform flows.” *River Res. Appl.* 28 (4): 418–428. https://doi.org/10.1002/rra.1564.

Nezu, I., and W. Rodi. 1985. “Experimental study on secondary currents in open channel flow.” In *Proc., 21st IAHR Biennial Congress*, 114–119. Beijing: International Association for Hydro-Environment Engineering and Research.

Nikuradse, J. 1926. “Turbulente Stromung im Innem des rechteckigen offenen Kanals.” [In German.] *Forschungsarbeiten* 281: 36–44.

Olsen, A., and B. Tullis. 2013. “Laboratory study of fish passage and discharge capacity in slip-lined, baffled culverts.” *J. Hydraul. Eng.* 139 (4): 424–432. https://doi.org/10.1061/(ASCE)HY.1943-7900.0000697.

Pavlov, D. S. 1999. *Structures assisting the migrations of non-salmonid fish: USSR*. FAO Fisheries Technical Paper No. 308, Rome: Food and Agriculture organization of the United Nations.

Pavlov, D. S., A. I. Lupandin, and M. A. Skorobogatov. 2000. “The effects of flow turbulence on the behavior and distribution of fish.” *J. Ichthyol.* 40 (2): 232–261.

Repogle, J. A. 1964. “Tractive-force distribution in sewers and channels.” Ph.D. thesis, Dept. of Civil Engineering, Univ. of Illinois.

Repogle, J. A., and V. T. Chow. 1966. “Tractive-force distribution in open channels.” *J. Hydraul. Div.* 92 (2): 169–191.

Schall, J. D., P. L. Thompson, S. M. Zerges, R. T. Kilgore, and J. L. Morris. 2012. *Hydraulic design of highway culverts*. FHWA-HIF-12-026. Washington, DC: Federal Highway Administration.

Sterling, M. 1998. “A study of boundary shear stress, flow resistance and the free overfall in open channels with a circular cross section.” Ph.D. thesis, School of Civil Engineering, Univ. of Birmingham.

Sterling, M., and D. W. Knight. 2000. “Resistance and boundary shear in circular conduits with flat beds running part full.” *Proc. Inst. Civ. Eng.* 142 (4): 229–240. https://doi.org/10.1680/wame.2000.142.4.229.

Tominaga, A., and I. Nezu. 1991. “Turbulent structure of shear flow with spanwise roughness heterogeneity.” In *Proc., Int. Symp. on Environmental Hydraulics*, 16–18. Rotterdam, Netherlands: A.A. Balkema.

Wang, H., and H. Chanson. 2018a. “Modelling upstream fish passage in standard box culverts: Interplay between turbulence, fish kinematics, and energetics.” *River Res. Appl.* 34 (3): 244–252. https://doi.org/10.1002/rra.3245.

Wang, H., and H. Chanson. 2018b. “On upstream fish passage in standard box culverts: Interactions between fish and turbulence.” *J. Ecohydraul.* 3 (1): 18–29. https://doi.org/10.1080/24705357.2018.1440183.

Wang, H., H. Chanson, P. Kern, and C. Franklin. 2016. “Culvert hydrodynamics to enhance upstream fish passage: Fish response to turbulence.” In *Proc., 20th Australasian Fluid Mechanics Conf., Australasian Fluid Mechanics Society*, edited by G. Ivey, S. Zhou, N. Jones, and S. Draper. Perth, WA, Australia: Australasian Fluid Mechanics Society.

Wang, H., W. Uys, and H. Chanson. 2018. “Alternative mitigation measures for fish passage in standard box culverts: Physical modelling.” *J. Hydro-environ. Res.* 19 (Mar): 214–223. https://doi.org/10.1016/j.jher.2017.03.001.

Wilkes, M. A., J. A. Webb, P. S. Pompeu, L. G. M. Silva, A. S. Vowles, C. F. Baker, P. Franklin, O. Link, E. Habit, and P. S. Kemp. 2018. “Not just a migration problem: Metapopulations, habitat shifts, and gene flow are also important for fishway science and management.” *River Res. Appl.* 35 (10): 1688–1696. https://doi.org/10.1002/rra.3320.

Wu, Y., Z. Liu, Y. Chen, and M. Li. 2018. “Investigation of velocity distribution and turbulence characteristics in subcritical circular open channel flows using a modified Reynolds stress model.” *J. Hydro-environ. Res.* 19 (Mar): 68–77. https://doi.org/10.1016/j.jher.2018.02.002.

Xie, Q. 1998. “Turbulent flows in non-uniform open channels: Experimental measurements and numerical modelling.” Ph.D. thesis, Dept. of Civil Engineering, Univ. of Queensland.